A singular value analysis of boundary layer control

Junwoo Lim[a] and John Kim[b]
Department of Mechanical and Aerospace Engineering, University of California at Los Angeles, Los Angeles, California 90095-1597

(Received 26 September 2003; accepted 24 February 2004; published online 30 April 2004)

Several approaches for boundary-layer control are analyzed from a linear system point of view. The singular value decomposition (SVD) is applied to the linearized Navier–Stokes system in the presence of control. The performance of control is examined in terms of the largest singular values, which represent the maximum disturbance energy growth ratio attainable in the linear system under control. It is shown that the maximum growth ratio is less in controlled systems than in the uncontrolled system only when control parameters are within a certain range of values. With opposition control, for example, when the detection plane is located too far away from the wall, the maximum energy growth ratio is larger, consistent with the results observed in direct numerical simulations. The SVD analysis of other controls also shows a similarity between the trend observed in the SVD analysis (linear) and that observed in direct numerical simulations (nonlinear), thus reaffirming the importance of linear mechanisms in the near-wall dynamics of turbulent boundary layers. The present study illustrates that the SVD analysis can be used as a guideline for designing controllers for drag reduction in turbulent boundary layers. © *2004 American Institute of Physics.* [DOI: 10.1063/1.1710522]

I. INTRODUCTION

There has been increased activity recently in developing efficient and robust controllers for viscous drag reduction in turbulent boundary layers. Many of these new approaches are quite different from the existing ones in that either they are directly utilizing modern control theory or they are derived from purely mathematical properties of the equations that govern the flow under investigation. Although turbulent flows are generally governed by nonlinear dynamics, some of these new approaches specifically target a linear mechanism that has been identified to be responsible for high-skin friction drag in turbulent boundary layers.[1–3]

Lately, the importance of linear mechanisms in wall-bounded turbulent flows has been well recognized. Butler and Farrell[4,5] investigated linearized Navier–Stokes equations in order to describe the formation mechanism of near-wall turbulence structures. They observed the so-called ''optimal'' disturbances,[6] which can grow significantly below the critical Reynolds number predicted by classical stability theory, before they eventually decay as predicted by the linear theory. This so-called transient growth can lead to subcritical transition to turbulence. They further showed that the shapes of optimal disturbances from the linearized flow model were similar to near-wall streamwise vortices in turbulent boundary layers, when a proper time scale was imposed in their linear analysis. It is worth mentioning that the transient growth of these optimal disturbances is due to the non-normality of the linearized Navier–Stokes equations, and hence it is a linear process.[7–9] Successful control aiming to alter this linear mechanism can be constructed to yield significant changes in turbulent boundary layers.[10]

The fact that a linear mechanism plays an important role in turbulent—and hence nonlinear—flows allows us to investigate the flow from a linear system theory point of view. In this study we apply the singular value decomposition (SVD) analysis to a few existing boundary-layer controllers in order to gain new insights into the mechanism by which these controllers are able to accomplish the viscous drag reduction in turbulent boundary layers. We will examine linear-quadratic-regulator (LQR) controllers that we have developed,[2,11] as well as the opposition control used by Choi *et al.*[12] Note that all of these methods have been designed to achieve a similar goal, i.e., suppressing the interactions between the near-wall streamwise vortices and the wall, in order to reduce skin-friction drag in turbulent boundary layers. Opposition control, which has been used as a reference against which many controllers have been compared,[13–15] is also used as a reference case in the present study. Although there have been some explanations as to how opposition control works, it is not yet completely understood, including how to determine the optimal location of the detection plane and why certain locations lead to an increase of turbulence and the skin-friction drag.

Most previous explanations for successful control schemes have been aimed at providing phenomenological interpretations, and have been induced from observations of controlled flow fields.[12,16–18] In this study, we investigate mathematical properties of the governing equations with control, in order to explain the observed behaviors of controlled flows. In particular, we shall investigate the linearized Navier–Stokes equations from the point of a linear system theory. The present approach allows us to examine the opti-

[a]Present address: Pittsburgh Supercomputing Center, 4400 Fifth Avenue, Pittsburgh, PA 15213.
[b]Author to whom correspondence should be addressed.

mal choice of control parameters and their performance at higher Reynolds numbers, which are normally too large to perform numerical simulations.

II. MATHEMATICAL FORMULATIONS

A. Linearized Navier–Stokes equations

In this study, we investigate turbulent channel flows, where the flow is statistically homogeneous in the streamwise (x) and the spanwise (z) directions. We first decompose the Navier–Stokes equations into linear and nonlinear parts. By representing the wall-normal velocity v and the wall-normal vorticity ω in terms of Fourier modes in the streamwise and the spanwise directions, the incompressible Navier–Stokes equations can be written in the following operator form:

$$\frac{\partial}{\partial t}\begin{bmatrix} v \\ \omega \end{bmatrix} = [\mathcal{A}]\begin{bmatrix} v \\ \omega \end{bmatrix} + \begin{bmatrix} \mathcal{N}_v \\ \mathcal{N}_\omega \end{bmatrix}, \tag{1}$$

where all nonlinear parts are lumped into $\mathcal{N}_v$ and $\mathcal{N}_\omega$. The operator $\mathcal{A}$ represents the linearized Navier–Stokes system operator defined as

$$[\mathcal{A}] = \begin{bmatrix} L_{os} & 0 \\ L_c & L_{sq} \end{bmatrix},$$

and the hat denotes a Fourier-transformed quantity. Here L_{os}, L_{sq}, and L_c represent the Orr–Sommerfeld, Squire, and linear coupling operators, respectively, and are defined as

$$\begin{aligned} L_{os} &= \Delta^{-1}\left(-\mathrm{i}k_x U\Delta + \mathrm{i}k_x \frac{d^2U}{dy^2} + \frac{1}{\mathrm{Re}}\Delta^2 \right), \\ L_{sq} &= -\mathrm{i}k_x U + \frac{1}{\mathrm{Re}}\Delta, \\ L_c &= -\mathrm{i}k_z \frac{dU}{dy}. \end{aligned} \tag{2}$$

Here, k_x and k_z are the streamwise and spanwise wave numbers, respectively, $\Delta = \partial^2/\partial y^2 - k_x^2 - k_z^2$, and U is the time-averaged mean velocity on which the linearized form is based. The Reynolds number Re is based on the wall-shear velocity, $u_\tau = \sqrt{\tau_w/\rho}$, and the channel half width h where $\tau_w = \nu dU/dy|_w$ is the mean shear stress at the wall, and ν and ρ denote the kinematic viscosity and the density, respectively. The superscript "+" denotes quantities nondimensionalized by ν and u_τ.

Investigating the role of linear mechanisms in the full Navier–Stokes equations can provide useful insights into the dynamics of the whole nonlinear system. For example, Kim and Lim[9] showed that when the linear coupling operator (L_c) was artificially removed from the nonlinear Navier–Stokes equations (referred to as a virtual flow), the channel flow became laminar at a Reynolds number that was normally large enough to maintain the flow turbulent. They postulated that opposition control could be viewed as a control strategy to reduce the effect of the linear coupling, since opposition control reduces spanwise variations of the wall-normal velocity in the near-wall region. This example illustrates that some control mechanisms can be analyzed from a linear system perspective.

It has been reported that the linear operator $\mathcal{A}$ is non-normal (i.e., not self-adjoint), and hence its eigenmodes are nonorthogonal to each other, thus allowing transient growth of disturbance energy even if all individual modes are stable and decay asymptotically.[4,7] More specifically, it has been shown that, due to this non-normality of the linearized Navier–Stokes system, an "optimal" disturbance (or perturbation) can grow up to $\mathcal{O}(\mathrm{Re}^2)$ in the transient time period, which is proportional to $\mathcal{O}(\mathrm{Re})$, possibly triggering nonlinear transition even below the critical Reynolds number predicted by classical linear stability theory.[4,7,8,19,20] Butler and Farrell[4] further illustrated that the shape of this optimal disturbance resembles near-wall streamwise vortices in wall-bounded turbulent flows. They also reported that when a proper turbulence time scale is imposed in their analysis, the spacing between high- and low-speed streaks induced by this optimal disturbance was close to that commonly observed in turbulent boundary layers. They postulated that those commonly observed organized turbulence structures in turbulent boundary layers are closely related to the same linear mechanisms.[5]

The optimal disturbance mentioned above is based on the linearized system, and the growth mechanism of such an optimal disturbance can be analyzed through a singular value decomposition of the system operator.[7] Furthermore, we have observed that the mean drag reduction in controlled boundary layers is a consequence of attenuated flow activities in the near-wall region, which is strongly influenced by the same linear mechanism. Therefore we postulate that the SVD analysis of the linearized Navier–Stokes system with control input can lead to new insights into various control schemes that have been used for drag reduction in turbulent boundary layers. With this postulation, we shall investigate the following form of the linearized Navier–Stokes equations for each wave-number pair:

$$\frac{\partial}{\partial t}\begin{bmatrix} v \\ \omega \end{bmatrix} = [\mathcal{A}]\begin{bmatrix} v \\ \omega \end{bmatrix}. \tag{3}$$

It should be emphasized, however, that the linearized Navier–Stokes equations are not sufficient in general to describe many features of turbulent boundary layers, including the self-sustaining mechanism of near-wall turbulence for which a nonlinear mechanism plays an essential role.[21]

B. State-space representation

The first step to apply the SVD analysis to a linear system is to formulate the governing equations in terms of the state-space representation as is done in the linear optimal controller design. The linearized Navier–Stokes equations with control input can be written in the following state-space representation:

$$\frac{d\mathbf{x}}{dt} = \mathbf{A}\mathbf{x} + \mathbf{B}\mathbf{u}, \tag{4}$$

$$\mathbf{u} = -\mathbf{K}\mathbf{x}, \tag{5}$$

where **x** and **u** are defined as

$$\mathbf{x} \equiv [v_1 \cdots v_{N-1} \quad \omega_1 \cdots \omega_{N-1}]^T,$$

$$\mathbf{u} \equiv [v_0 \quad v_N]^T.$$

Here, we use the collocation matrix approach used by Bewley and Liu.[22] Detailed derivations and explanations for the matrices **A** and **B** can be found in Bewley and Liu[22] and Lim.[11] The vector **x** represents a ''state'' of the system, and it consists of the wall-normal velocity and wall-normal vorticity at each collocation point. The subscripts denote collocation points in the wall-normal direction (0 and N correspond to the upper and lower wall, respectively). The other vector **u** represents ''control,'' which is blowing and suction at the wall in the present study. Equation (4) represents a state equation inside the flow domain, which is being forced by the control input at the boundary of the domain.

In standard optimal control theory, the control gain matrix **K** is usually constructed such that the controlled system is linearly stable and a certain cost function is minimized. Linear-quadratic-regulator (LQR) minimizes a quadratic form of a cost function such as

$$\mathcal{J} = \int_0^\infty (\gamma \mathbf{x}^* \mathbf{Q} \mathbf{x} + \mathbf{u}^* \mathbf{R} \mathbf{u}) dt, \tag{6}$$

where the superscript * denotes conjugate transpose and γ is a control parameter. The matrices **Q** and **R**, respectively, represent a particular form of the control objective and how the cost of control should be accounted for. A large weighting on the cost of control (small γ) signifies a high cost of control, and vice versa. The optimal control input **u** minimizing the cost function is found in the following form:

$$\mathbf{u}(t) = -\mathbf{K}\mathbf{x}(t) = -\mathbf{R}^{-1}\mathbf{B}^*\mathbf{P}\mathbf{x}(t), \quad t \geqslant 0,$$

where **P** is a unique self-adjoint matrix that satisfies the algebraic Riccati equation:

$$\mathbf{A}^*\mathbf{P} + \mathbf{P}\mathbf{A} - \mathbf{P}\mathbf{B}\mathbf{R}^{-1}\mathbf{B}^*\mathbf{P} + \gamma\mathbf{Q} = 0. \tag{7}$$

Although solving the above equations is numerically challenging, many algorithms[23,24] and numerical packages such as SLICOT[25] and MATLAB's *Control System Toolbox*[26] are available.

The control gain matrix **K** for opposition control can be easily constructed once the detection-plane location is chosen. Note that **K** can be expressed in terms of two submatrices:

$$\mathbf{K} \equiv [\mathbf{K}_v \quad \mathbf{K}_\omega].$$

Each submatrix of the control-gain matrix **K** represents a portion of a feedback law using the wall-normal velocity and wall-normal vorticity, respectively. Then, $\mathbf{K}_\omega$ is a $2 \times (N-1)$ zero matrix, whereas $\mathbf{K}_v$ is a $2 \times (N-1)$ matrix, defined as

$$\mathbf{K}_v \equiv \begin{bmatrix} 0 & \cdots & 0 & 1 & 0 & \cdots & \cdots & \cdots & 0 \\ 0 & \cdots & \cdots & \cdots & 0 & 1 & 0 & \cdots & 0 \end{bmatrix},$$

when control is applied on both walls. Recall that $v_{wall} = -v(y_d^+)$ for opposition control (see Fig. 1), and therefore, except for the two elements that correspond to the detection planes, all elements in the gain matrix are zero. Unlike the optimal control, opposition control neither guarantees that the controlled system will be linearly stable, nor minimizes any cost function. Also note that opposition control modifies the L_{os} portion of **A** only.

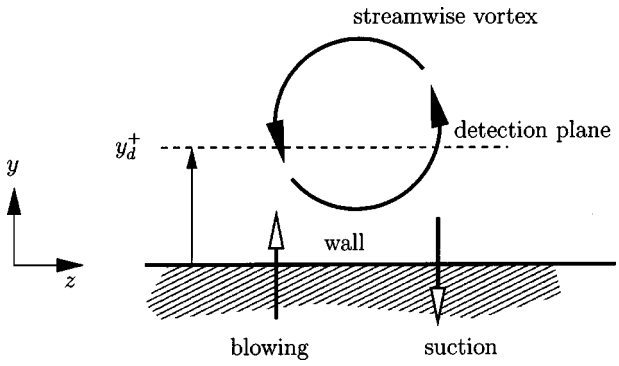

FIG. 1. A schematic diagram for opposition control.

By combining Eqs. (4) and (5), the system equation for controlled cases is given as $\dot{\mathbf{x}} = (\mathbf{A} - \mathbf{B}\mathbf{K})\mathbf{x}$. For uncontrolled cases, **K** is zero and the system equation simply becomes $\dot{\mathbf{x}} = \mathbf{A}\mathbf{x}$.

C. Singular value decomposition

The traditional eigenvalue analysis, which predicts whether a linear system is stable or unstable based on the eigenvalues of the system, is inadequate in explaining the transient growth of the kinetic energy of certain disturbances in an otherwise stable system. Instead, the transient growth can be analyzed by applying the SVD analysis to the system operator,[7] by which the amplification factor of the optimal disturbance can be determined. We hypothesize that the SVD analysis is also applicable for examining the performance of controllers for turbulent boundary layers. Effective controllers must reduce the non-normality of the flow system, since it is also believed to be responsible for sustaining near-wall turbulence structures (which in turn are responsible for high skin-friction drag in turbulent boundary layers), and therefore the SVD analysis should reveal reduction of singular values representing the transient energy growth in the controlled system.

To analyze the transient energy growth, we consider the ratio of the kinetic energy of a disturbance at a given time (τ) to the disturbance energy at $t = 0$. In this study, we use a procedure similar to that used by Reddy and Henningson,[7] but different approaches (e.g., Butler and Farrell,[4] Bewley and Liu[22]) should lead to the same results. We consider the growth ratio function defined as

$$G(\tau) = \sup_{\mathbf{x}(\cdot,0) \neq 0} \frac{\|\mathbf{x}(\tau)\|^2}{\|\mathbf{x}(0)\|^2}, \tag{8}$$

where

$$\|\mathbf{x}\|^2 \equiv \int_{-1}^{1} \left[v^* v + \frac{1}{k_x^2 + k_z^2} \left(\frac{\partial v^*}{\partial y} \frac{\partial v}{\partial y} + \omega^* \omega \right) \right] dy,$$

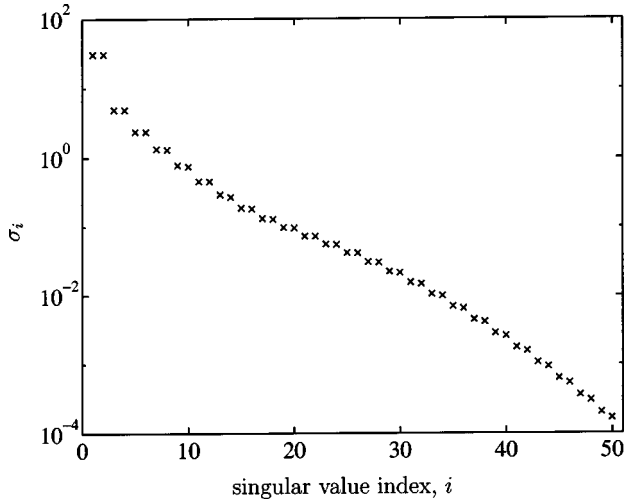

FIG. 2. The first 50 singular values of (Re=180, $\tau^+=80$) case ($k_x=0$, $k_z=10.5$).

and τ is the given time mentioned above. The quantity $\|\mathbf{x}\|^2$ represents the kinetic energy of $\mathbf{x}$ and can be expressed as $\|\mathbf{x}(t)\|^2=\mathbf{x}^*(t)\mathbf{Q}\mathbf{x}(t)$, where the Hermitian matrix $\mathbf{Q}$ is defined in terms of an inner product in discrete space with sufficient grid points.[7,22] The matrix $\mathbf{Q}$ can be further decomposed in the form $\mathbf{Q}=\mathbf{F}^*\mathbf{F}$, where $\mathbf{F}^*$ is the Hermitian conjugate of $\mathbf{F}$. The solution of the system equation is simply given by $\mathbf{x}(t)=\exp[(\mathbf{A}-\mathbf{BK})t]\mathbf{x}(0)$. It follows that

$$\|\mathbf{x}(t)\|^2=\mathbf{x}^*(t)\mathbf{F}^*\mathbf{F}\mathbf{x}(t)$$
$$=\|\mathbf{F}\mathbf{x}(t)\|_2^2=\|\mathbf{F}\exp[(\mathbf{A}-\mathbf{BK})t]\mathbf{x}(0)\|_2^2, \quad (9)$$

where $\|\cdot\|_2$ represents the 2-norm (Euclidian norm). Combining Eqs. (8) and (9), we obtain the growth ratio at τ as

$$G(\tau)=\sup_{\mathbf{x}(\cdot,0)\neq 0}\frac{\|\mathbf{F}\exp[(\mathbf{A}-\mathbf{BK})\tau]\mathbf{x}(0)\|_2^2}{\|\mathbf{F}\mathbf{x}(0)\|_2^2}$$
$$=\sup_{\mathbf{x}(\cdot,0)\neq 0}\|\mathbf{F}\exp[(\mathbf{A}-\mathbf{BK})\tau]\mathbf{F}^{-1}\|_2^2. \quad (10)$$

The 2-norm of a matrix can be easily computed from the SVD of the matrix. Typical SVD subroutines provide a diagonal matrix Σ and two orthogonal matrices $\mathbf{U}$ and $\mathbf{V}$, with which the original matrix can be expressed in the following form:

$$\mathbf{U}^H\mathbf{A}\mathbf{V}=\mathbf{\Sigma}, \quad (11)$$

where the superscript H denotes a Hermitian matrix, and the column vectors of $\mathbf{V}$ and $\mathbf{U}$ are referred to as right and left singular vectors, respectively. The diagonal elements of Σ are the singular values (σ's), which represents the two-norm ratio of corresponding column vectors of $\mathbf{V}$ and $\mathbf{U}$. In wall-bounded shear flows, only a few singular values are larger than one, as indicated in Fig. 2, implying that only a few particular disturbances can have the transient growth. The largest σ value represents the maximum energy growth ratio at τ, and the corresponding column vectors of $\mathbf{U}$ and $\mathbf{V}$ are the flow field at τ and the initial flow field, respectively. In other words, the initial flow field V_1 evolves in time τ to become U_1 with the growth ratio $G(\tau)=\sigma_1$, where σ_1 is the largest singular value. Note that the singular vectors are orthogonal to each other (both $\mathbf{U}$ and $\mathbf{V}$ are orthogonal matrices), and each singular vector can be expressed in terms of a combination of all eigenvectors.

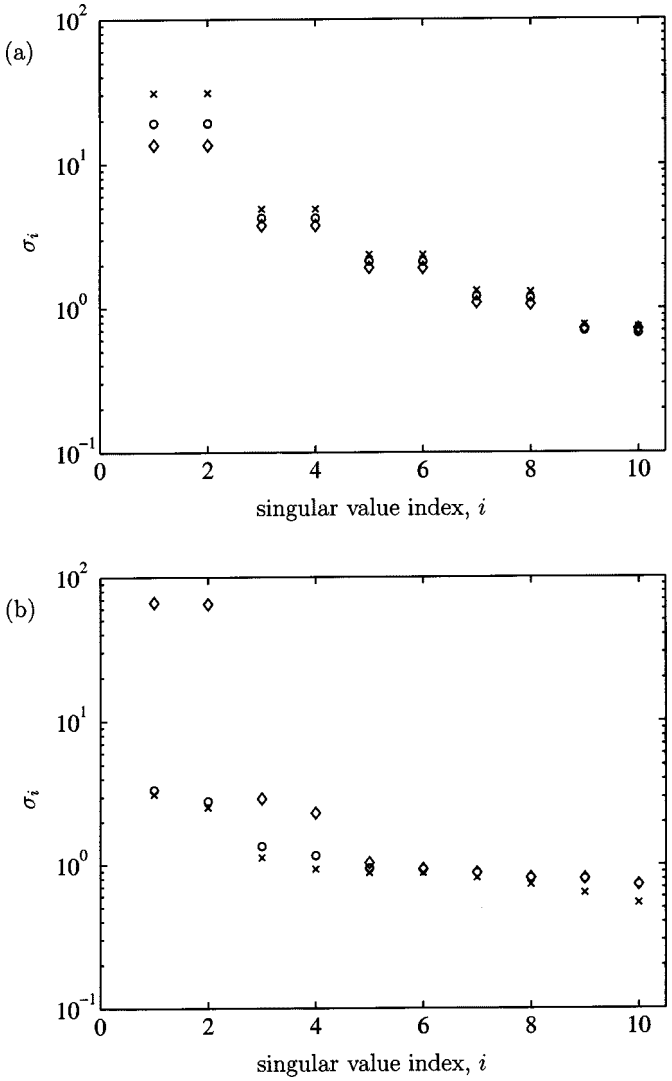

FIG. 3. The first 10 singular values with and without opposition control: (a) ($k_x=0$, $k_z=10.5$); (b) ($k_x=3$, $k_z=0$). For all cases, Re=180 and $\tau^+=80$. ×, No control; ○, $y_d^+=10$; ◇, $y_d^+=20$.

The singular vector V_1 corresponding to the largest $G(\tau)$ for all wave-number pairs is the ''optimal'' disturbance. The term ''optimal'' was originally chosen in the sense that this disturbance would have the largest (optimal) transient growth.[4] In a turbulent (hence nonlinear) flow environment, the evolution of this disturbance represents the most probable—at least linearly—scenario to grow and survive in the disruptive environment. In a turbulent flow environment, the given time scale τ plays an important role in determining the ''optimal'' disturbance. The time scale that was ''globally'' optimal for the maximum energy growth was found to be relatively large [$\sim\mathcal{O}(\mathrm{Re})$] and it was argued that such an ''optimal'' disturbance could not attain its potentially maximum state as nonlinear activities constantly disrupt the linear process.[5] Butler and Farrell[5] used the eddy turnover time in

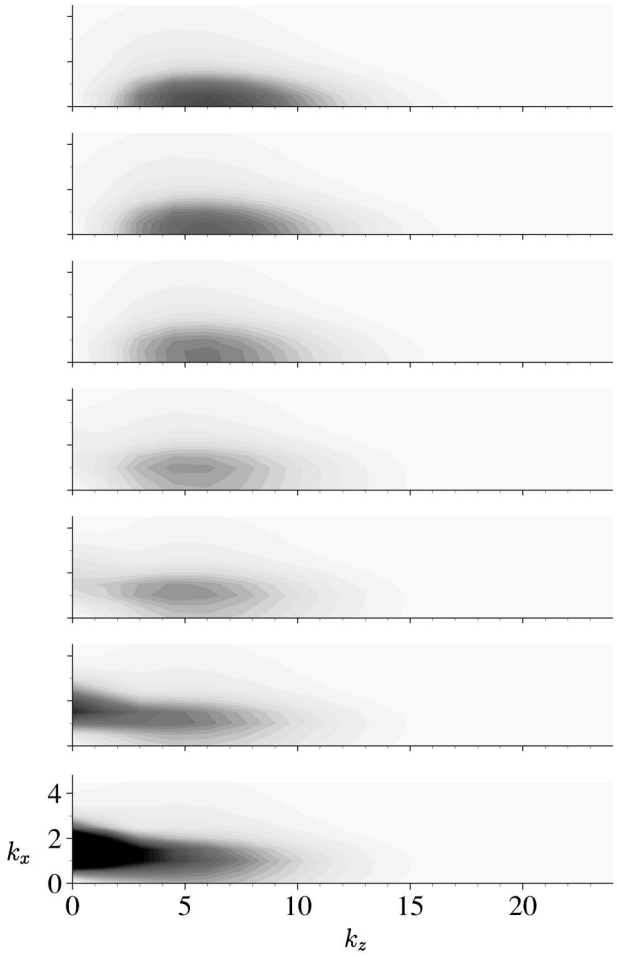

FIG. 4. Contours of $G(\tau)$ with various detection-plane locations. Darker area indicates the larger $G(\tau)$. Re=100 and $\tau^+=80$. From top to bottom, no control, $y_d^+=5.8$, 9.6, 14.2, 16.8, 19.6, and 25.9, respectively.

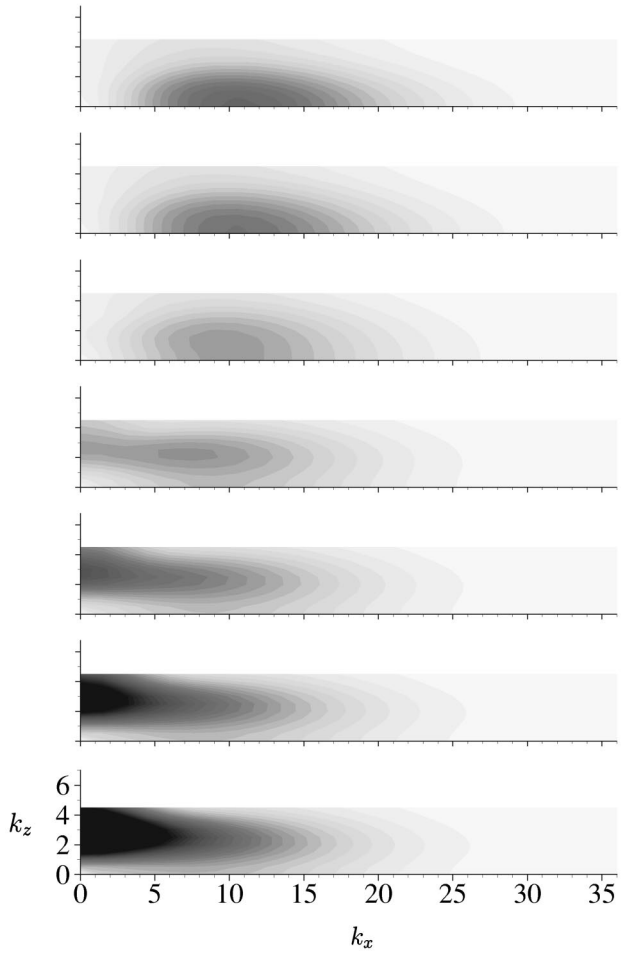

FIG. 5. See the caption of Fig. 4. Re=180 and $\tau^+=80$. From the top frame, no control, $y_d^+=5.3$, 10.4, 15.3, 17.1, 19.0, and 21.0, respectively.

the near-wall region, approximately $t^+=80$, for their τ, which resulted in the optimal disturbance similar to those observed in turbulent boundary layers.

In the following sections, we will apply the SVD analysis to the channel flow system with various controls. By comparing the largest singular values for the energy growth ratio for different control parameters, we will investigate the performance of each control. We mention here in passing that sufficiently fine resolution in the wall-normal direction must be used in order to obtain accurate values of $G(\tau)$ in controlled flows. This is because, unlike uncontrolled flows where contributions to $G(\tau)$ from higher eigenmodes are negligibly small,[7] it was found that $G(\tau)$ in controlled flows is sensitive to the wall-normal resolution, indicating that contributions from the higher eigenmodes are not negligible and hence must be resolved properly.

III. RESULTS

A. Energy growth ratio $G(\tau)$

The singular values representing the disturbance energy growth ratio with and without opposition control for a couple of wave-number pairs are shown in Fig. 3 as an example. Note that the largest singular value $[=G(\tau)]$ is reduced for one wave-number pair (a), while the same opposition control increases the energy growth ratio for the other wave-number pair (b).

Contours of $G(\tau)$ for all wave-number pairs are plotted in Figs. 4–6. The contour plots on top for each figure correspond to the uncontrolled case, where the maximum $G(\tau)$ occurs on the $k_x=0$ axis. Note that the length scale in the spanwise direction for the maximum $G(\tau)$ for the uncontrolled case is approximately equal to that of the wall-layer streaks.[5] With opposition control, the maximum $G(\tau)$ occurs at different wave-number pairs, depending on the choice of y_d^+. The maximum value of $G(\tau)$ decreases when y_d^+ is within a certain range, whereas it increases drastically when y_d^+ becomes too large. It is interesting to note that the maximum $G(\tau)$ occurs on the $k_z=0$ axis when y_d^+ is too large.

The maximum value of $G(\tau)$ as a function of y_d^+ for three different Re's are shown in Fig. 7. As Re increases, the optimal range moves closer to the wall. Although the shift amount seems insignificant (from $y_d^+=15$ to $y_d^+=10$ as Re $=100$ increases to Re=395), the y_d^+ that causes significant increase in G also moves closer to the wall as Re increases, thus narrowing the optimal range of y_d^+ at high Re. Also the reduction amount of $G(\tau)$ slightly decreases as Re increases. Chang *et al.*[18] performed large-eddy simulations (LES) for

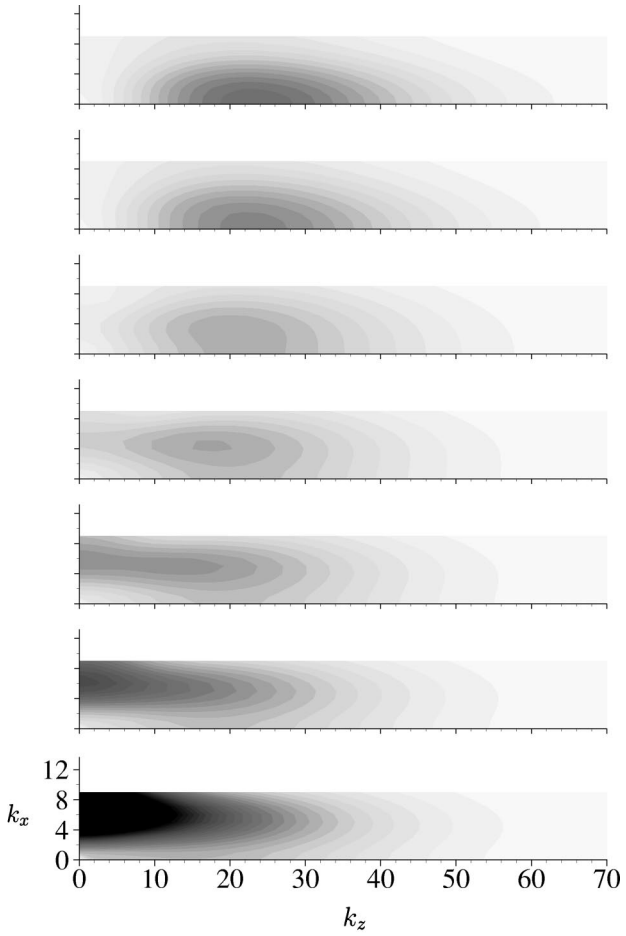

FIG. 6. See the caption of Fig. 4. Re=395 and $\tau^+=80$. From the top frame, no control, $y_d^+=5.8$, 10.6, 13.0, 14.2, 15.5, and 18.3, respectively.

several Reynolds numbers to show that both the drag reduction amount and the optimal y_d^+ for the maximum drag reduction decreased as Re was increased (from 48% drag reduction with $y_d^+\approx16$ to 18% with $y_d^+\approx13$, as Re=80 was increased to Re=720). It is important to recognize that the SVD analysis of opposition control led to the same trend as

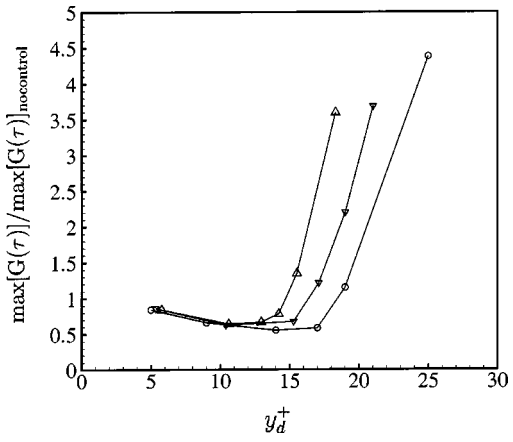

FIG. 7. The largest $G(\tau)$ under various conditions. ○, Re=100; ▽, Re =180; △, Re=395.

TABLE I. Largest $G(\tau)$ and corresponding length scales in wall units.

Re		No control	$y_d^+=y_{\text{opt}}^+$
100	$G(\tau)$	38.1	21.0
	(l_x^+,l_z^+)	(∞,105)	(630,125)
180	$G(\tau)$	30.7	19.2
	(l_x^+,l_z^+)	(∞,108)	(646,126)
395	$G(\tau)$	27.5	17.7
	(l_x^+,l_z^+)	(∞,108)	(620,118)
590	$G(\tau)$	27.7	17.5
	(l_x^+,l_z^+)	(∞,104)	(618,123)

the LES of opposition control, reaffirming the notion that much can be learned from a linear analysis of the nonlinear flow.

The length scales associated with optimal disturbances with opposition control appear to remain unchanged over Re, as is the case without the control, although they are quite different. Table I lists the length scales corresponding to optimal disturbance for uncontrolled and for the case of $G(\tau)$ reduced maximally with $y_d^+=y_{opt}^+$, where y_{opt}^+ indicates the detection location for the smallest $G(\tau)$. For Re $=100-590$, the optimal disturbance occurs near $l_x^+=600-650$ and $l_z^+\approx120$. When $y_d^+\gg y_{opt}^+$, $G(\tau)$ increases significantly, the maximum of which always occurs on the $k_z=0$ axis.

The SVD analysis can be also applied to other control design methods. Figure 8 shows the maximum $G(\tau)$ with different γ in an LQR design (minimizing $\mathbf{x}^*\mathbf{x}$). It is seen that a proper range of γ exists ($\gamma=0$ corresponds to no control) for this particular design: $10^{-5}\leqslant\gamma\leqslant10^{-4}$ will produce the most effective control. Note that the range of effective γ depends on the specific choice of LQR design parameters such as the cost function. Also, there are many other factors that can influence the performance of an LQR control.[3,11] Nonetheless, the SVD analysis provides a good initial guess for the trial-and-error procedure of the LQR design.

The maximum singular values for well-controlled cases are smaller than that of the uncontrolled case. In Fig. 9, a few singular values with the above LQR design are compared to those with opposition control (with the optimal detection plane). Also shown are the results obtained by applying the

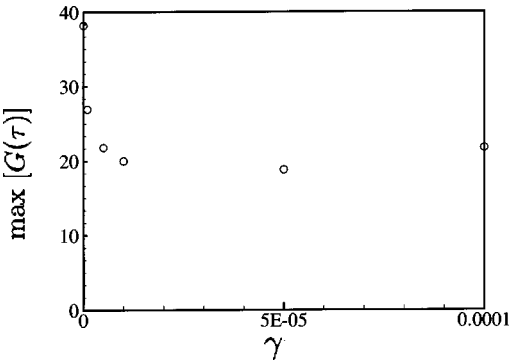

FIG. 8. The largest $G(\tau)$ with different γ (Re=100, minimizing $\mathbf{x}^*\mathbf{x}$).

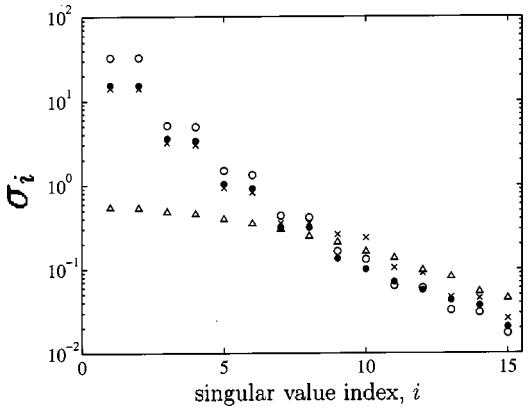

FIG. 9. Singular values in a turbulent channel with different controllers: ○, no control; ●, opposition control; ×, LQR control; △, virtual flow. This is for the case of ($k_x=0$, $k_z=6.0$), corresponding to $\lambda_z^+\approx 100$, and Re=100.

SVD analysis to the virtual flow investigated by Kim and Lim,[9] in which the linear coupling term between the Orr–Sommerfeld and the Squire equations was artificially removed. Note in particular that all singular values for the virtual flow are less than one, implying that no transient growth is possible in the virtual flow. Singular values for other wave-number pairs show a similar trend. From the distribution of these singular values, one would expect that the virtual flow would be most effective in reducing the skin-friction drag in turbulent boundary layers.

B. Turbulent flow control

In order to examine the applicability of the SVD analysis, which is based on the linearized Navier–Stokes equations, to fully nonlinear turbulent flows, we applied these controllers to direct numerical simulations of a turbulent channel flow at the same Re. All calculations were performed in the same manner described in Kim *et al.*,[27] except for the required modification due to imposed control.

Figure 10 shows the time evolution of mean skin-friction drag in the channel with the LQR control with various γ shown in Fig. 8. These results (nonlinear) are consistent with

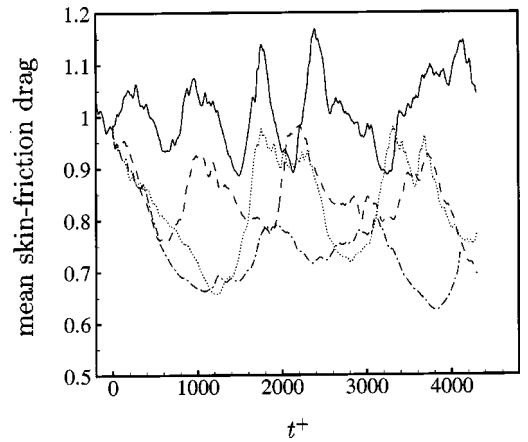

FIG. 10. Mean skin-friction drag history with different γ for an LQR control design (Re=100, minimizing $\mathbf{x}^*\mathbf{x}$). ——, No control; — — —, $\gamma=10^{-5}$; —·—·—·—, $\gamma=5\times10^{-5}$; · · · ·, $\gamma=10^{-4}$.

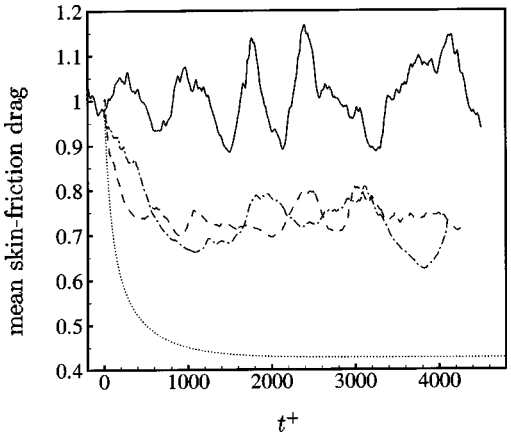

FIG. 11. Mean skin-friction drag history with various control methods (Re=100). ——, No control; — — —, opposition control ($y_d^+\approx 15$), —·—·—·—, LQR control ($\gamma=5\times10^{-5}$, minimizing $\mathbf{x}^*\mathbf{x}$); · · · ·, virtual flow.

the SVD analysis (linear). For different initial conditions (not shown here), $\gamma=5\times10^{-5}$ sometimes produced no more drag reduction than other choices, but it was observed that the optimal γ was always between 10^{-5} and 10^{-4}.

In Fig. 11, various controllers are compared in turbulent simulations. Note that the case without the linear coupling term (virtual flow) results in complete laminarization, consistent with the SVD analysis. Other cases are also consistent with the SVD analysis, demonstrating that the SVD analysis is a viable tool in predicting the performance of a controller in the nonlinear turbulent channel flow. It should be pointed out that these simulations were performed at an extremely low Reynolds number, and extending these results to much high Reynolds number flows must be done with some care. In this regard, it is worth mentioning the LES results by Chang *et al.*[18] The performance of opposition control at higher Reynolds numbers observed in their LES is consistent with the present SVD analysis, thus indirectly validating the application of the present SVD analysis, at least for opposition control, to higher Reynolds numbers.

IV. DISCUSSION

The application of the SVD analysis to the linearized flow system with control input provides useful information on the performance of the control, without carrying out actual nonlinear simulations. Although a straightforward application of the SVD to various controllers has proven to be useful, there are many issues to be addressed in order to apply the SVD analysis to more general control situations. Some of these issues are discussed below.

The mean velocity profile, upon which the nonlinear Navier–Stokes equations are linearized, changes due to control, and may affect the performance of the control. In fact, the difference between mean profiles in uncontrolled and controlled flows becomes larger when the control is more effective. Therefore, at some point during control, it is useful to re-examine the optimal choice of control parameters for the modified mean profile. Such ''gain scheduling'' is a common practice in control design.[3] In some sense, this is an

attempt to indirectly account for the nonlinearity (by which the mean velocity is modified) that is ignored in the linearized Navier–Stokes system. To apply the SVD analysis to control with gain-scheduling, however, a variable τ has to be introduced as control is applied. It is unclear at this point whether the same τ in wall units is still valid as the drag is reduced significantly, since the turbulence activity is also significantly reduced and the resulting wall-shear velocity may not be the proper velocity scale. As Butler and Farrell[5] pointed out, the selection of proper τ, through which a nonlinear effect is accounted for, is crucial in applying the linear analysis to nonlinear flows. It was found that the dependence of $G(\tau)$ on τ was greater for high streamwise wave-numbers, while $G(\tau)$ is large for low streamwise wave-numbers, thus indicating that the maximum value of $G(\tau)$ is relatively insensitive to the choice of τ. Nevertheless, it would be worth trying the same approach employed by Butler and Farrell[5] to find the eddy turnover time as the mean velocity evolves with control.

We have observed that the maximum value of $G(\tau)$ decreases as Re increases, suggesting that the linear mechanism responsible for the transient growth diminishes at high Re. Thus, if this linear mechanism is primarily responsible for the drag reduction, the effectiveness of the control methods discussed in the present study may also decrease at high Re. Such a trend for opposition control has been reported by Chang *et al.*[18] However, the drag reduction may have been affected not only by the reduction of $G(\tau)$, but also by reduction of contributions from other linear mechanisms. Moreover, the effect of linear control on nonlinear mechanisms is not yet well understood. As such it is not clear at this point how these controllers aiming to reduce linear mechanisms in turbulent boundary layers will perform in high Reynolds number flows.

V. CONCLUSION

We have shown that boundary-layer control can be analyzed from a linear system perspective. The SVD analysis provided new insights into opposition control and other linear controls regarding their capability of attenuating the transient growth of disturbances in turbulent boundary layers.

The SVD analysis of opposition control indicated existence of an optimal range of the detection plane. It also showed that opposition control using detection planes too far away from the wall could enhance the growth of certain disturbances, consistent with observations in DNS/LES. Similarly, an optimal range of the weight parameter in LQR control may exist for some designs.

The trends observed from the SVD analysis were similar to those observed in DNS or LES of drag-reduced turbulent flows, illustrating that the linear system model can describe an important part of the near-wall dynamics and that it can be used as a guideline for various control designs for drag reduction. It could be used, for example, in optimizing control parameters without actually performing expensive nonlinear computations. Other issues, such as the effects of using the evolving mean flow as control applied to a nonlinear flow system (also known as gain scheduling), and high Reynolds number limitations, will be investigated through the SVD analysis in future research.

ACKNOWLEDGMENTS

We are grateful to Professor Jason Speyer for useful discussions during the course of this work. This work has been supported by the Air Force Office of Scientific Research (F49620-00-10105, Dr. Marc Jacobs and Dr. Belinda King; F49620-03-1-0038, Dr. Thomas Beutner). The computer time provided by NSF NPACI Centers (Pittsburgh Supercomputing Center in particular for J.L.) is also gratefully acknowledged.

[1] S. S. Joshi, J. L. Speyer, and J. Kim, "A systems theory approach to the feedback stabilization of infinitesimal and finite-amplitude disturbances in plane Poiseuille flow," J. Fluid Mech. **332**, 157 (1997).
[2] K. H. Lee, L. Cortelezzi, J. Kim, and J. L. Speyer, "Application of reduced-order controller to turbulent flows for drag reduction," Phys. Fluids **13**, 1321 (2001).
[3] M. Högberg, T. R. Bewley, and D. S. Henningson, "Relaminarization of Re_τ=100 turbulence using gain scheduling and linear state-feedback control," Phys. Fluids **15**, 3572 (2003).
[4] K. M. Butler and B. F. Farrell, "Three-dimensional optimal perturbations in viscous shear flow," Phys. Fluids A **4**, 1637 (1992).
[5] K. M. Butler and B. F. Farrell, "Optimal perturbations and streak spacing in wall-bounded turbulent shear flow," Phys. Fluids A **5**, 774 (1993).
[6] From a control point of view, this is actually the "worst" disturbance, and therefore we use this commonly used term in quotes to avoid confusion with optimal control. See Sec. II C for further discussion.
[7] S. C. Reddy and D. S. Henningson, "Energy growth in viscous channel flows," J. Fluid Mech. **252**, 209 (1993).
[8] L. N. Trefethen, A. E. Trefethen, S. C. Reddy, and T. A. Driscoll, "Hydrodynamic stability without eigenvalues," Science **261**, 578 (1993).
[9] J. Kim and J. Lim, "A linear process in wall-bounded turbulent shear flows," Phys. Fluids **12**, 1885 (2000).
[10] J. Kim, "Control of turbulent boundary layers," Phys. Fluids **15**, 1093 (2003).
[11] J. Lim, "A linear control in turbulent boundary layers," Ph.D. dissertation, University of California at Los Angeles, 2003.
[12] H. Choi, P. Moin, and J. Kim, "Active turbulence control for drag reduction in wall-bounded flows," J. Fluid Mech. **262**, 75 (1994).
[13] C. Lee, J. Kim, D. Babcock, and R. Goodman, "Application of neural networks to turbulence control for drag reduction," Phys. Fluids **9**, 1740 (1997).
[14] C. Lee, J. Kim, and H. Choi, "Suboptimal control of turbulent channel flow for drag reduction," J. Fluid Mech. **358**, 245 (1998).
[15] T. R. Bewley, P. Moin, and R. Temam, "DNS-based predictive control of turbulence: An optimal benchmark for feedback algorithms," J. Fluid Mech. **447**, 179 (2001).
[16] E. P. Hammond, T. R. Bewley, and P. Moin, "Observed mechanisms for turbulence attenuation and enhancement in opposition-controlled wall-bounded flows," Phys. Fluids **10**, 2421 (1998).
[17] R. D. Prabhu, S. S. Collis, and Y. Chang, "The influence of control on proper orthogonal decomposition of wall-bounded turbulent flows," Phys. Fluids **13**, 520 (2001).
[18] Y. Chang, S. S. Collis, and S. Ramakrishnan, "Viscous effects in control of near-wall turbulence," Phys. Fluids **14**, 4069 (2002).
[19] B. F. Farrell and P. J. Ioannou, "Optimal excitation of three-dimensional perturbations in viscous contant shear flow," Phys. Fluids A **5**, 1390 (1993).
[20] B. Bamieh and M. Dahleh, "Energy amplification in channel flows with stochastic excitation," Phys. Fluids **13**, 3258 (2001).
[21] J. M. Hamilton, J. Kim, and F. Waleffe, "Regeneration mechanisms of near wall turbulence structures," J. Fluid Mech. **287**, 317 (1995).
[22] T. R. Bewley and S. Liu, "Optimal and robust control and estimation of linear paths to transition," J. Fluid Mech. **365**, 305 (1998).
[23] W. F. Arnold and A. J. Laub, "Generalized eigenproblem algorithms and

software for algebraic Riccati equations,'' Proc. IEEE **72**, 1746 (1984).
[24]L. Dieci, ''Numerical integration of the differential Riccati equation and some related issues,'' SIAM (Soc. Ind. Appl. Math.) J. Numer. Anal. **29**, 781 (1992).
[25]P. Benner, V. Mehrmann, V. Sima, S. Van Huffel, and A. Varga, ''SLICOT—A Subroutine Library in Systems and Control Theory,'' NICONET Report **97-3** (1997) (available online, http://www.win.tue.nl/niconet/NIC2/slicot.html).
[26]D. K. Frederick and J. H. Chow, *Feedback Control Problems: Using MATLAB and the Control System Toolbox* (Brooks/Cole, Pacific Grove, 2000).
[27]J. Kim, P. Moin, and R. K. Moser, ''Turbulence statistics in fully developed channel flow at low Reynolds number,'' J. Fluid Mech. **177**, 133 (1987).